Cosmological data favor Galileon ghost condensate over ΛCDM

Simone Peirone[1], Giampaolo Benevento[2,3], Noemi Frusciante[4], Shinji Tsujikawa[5]

[1]*Institute Lorentz, Leiden University, PO Box 9506, Leiden 2300 RA, The Netherlands*

[2]*Dipartimento di Fisica e Astronomia "G. Galilei",*
Università degli Studi di Padova, via Marzolo 8, I-35131, Padova, Italy

[3]*INFN, Sezione di Padova, via Marzolo 8, I-35131, Padova, Italy*

[4]*Instituto de Astrofísica e Ciências do Espaço, Faculdade de Ciências da Universidade de Lisboa,*
Edifício C8, Campo Grande, P-1749016, Lisboa, Portugal

[5]*Department of Physics, Faculty of Science, Tokyo University of Science,*
1-3, Kagurazaka, Shinjuku-ku, Tokyo 162-8601, Japan

(Dated: October 1, 2019)

We place observational constraints on the Galileon ghost condensate model, a dark energy proposal in cubic-order Horndeski theories consistent with the gravitational-wave event GW170817. The model extends the covariant Galileon by taking an additional higher-order field derivative X^2 into account. This allows for the dark energy equation of state w_{DE} to access the region $-2 < w_{DE} < -1$ without ghosts. Indeed, this peculiar evolution of w_{DE} is favored over that of the cosmological constant Λ from the joint data analysis of cosmic microwave background (CMB) radiation, baryonic acoustic oscillations (BAOs), supernovae type Ia (SNIa) and redshift-space distortions (RSDs). Furthermore, our model exhibits a better compatibility with the CMB data over the Λ-cold-dark-matter (ΛCDM) model by suppressing large-scale temperature anisotropies. The CMB temperature and polarization data lead to an estimation for today's Hubble parameter H_0 consistent with its direct measurements at 2σ. We perform a model selection analysis by using several methods and find a statistically significant preference of the Galileon ghost condensate model over ΛCDM.

PACS numbers:

I. INTRODUCTION

The late-time cosmic acceleration has been firmly confirmed by several independent observations including SNIa [1–3], CMB [4–6], and BAOs [7–9]. Although the cosmological constant Λ is the simplest candidate for the source of this phenomenon, it is generally plagued by the problem of huge difference between the observed dark energy scale and the vacuum energy associated with particle physics [10]. In the ΛCDM model, there have been also tensions for today's Hubble expansion rate H_0 constrained from the Planck CMB data [5] and its direct measurements at low redshifts [11].

In the presence of a scalar field ϕ, the negative pressure arising from its potential or nonlinear kinetic energy can drive the cosmic acceleration. If we allow for derivative interactions and nonminimal couplings to gravity, Horndeski theories [12] are the most general scalar-tensor theories with second-order equations of motion ensuring the absence of Ostrogradski instabilities [13, 14]. The gravitational-wave event GW170817 [15] together with its electromagnetic counterpart [16] show that the speed of gravity c_t is close to that of light with the relative difference $\sim 10^{-15}$. If we strictly demand that $c_t = 1$, the Horndeski Lagrangian is of the form $L_H = G_4(\phi)R + G_2(\phi, X) + G_3(\phi, X)\Box\phi$, where R is the Ricci scalar, G_4 is a function of ϕ, and G_2, G_3 depend on both ϕ and $X = \partial_\mu\phi\partial^\mu\phi$ [17–21].

Theories with the nonminimal coupling $G_4(\phi)R$ include $f(R)$ gravity and Brans-Dicke theories, but we have not yet found any observational signatures for supporting nonminimally coupled dark energy models over the cosmological constant. The minimally coupled quintessence and k-essence with the Lagrangian $L = M_{pl}^2 R/2 + G_2(\phi, X)$, where M_{pl} is the reduced Planck mass, predicts $w_{DE} > -1$ under the absence of ghosts, but there has been no significant observational evidence that these models are favored over ΛCDM.

The cubic-order Horndeski Lagrangian $G_3(\phi, X)\Box\phi$ allows an interesting possibility for realizing $w_{DE} < -1$ without ghosts. In cubic Galileons with the Lagrangian $L = M_{pl}^2 R/2 + a_1 X + 3a_3 X\Box\phi$ [22, 23], where a_1 and a_3 are constants, there exists a tracker solution along which $w_{DE} = -2$ during the matter era [24]. This behavior of w_{DE} is in tension with the joint data analysis of SNIa, CMB, and BAO [25]. The dominance of cubic Galileons as a dark energy density at low redshifts also leads to the enhancement of perturbations incompatible with measurements of the cosmic growth history [26, 27].

The above problems of Galileons are alleviated by taking a scalar potential $V(\phi)$ [28, 29] or a nonlinear term of X in $G_2(\phi, X)$ into account [30]. In particular, the latter model can lead to w_{DE} in the range $-2 < w_{DE} < -1$. Moreover, the Galileon is not necessarily the main source for late-time cosmic acceleration in this case, so it should be compatible with cosmic growth measurements. In this letter, we show that the cubic Galileon model with a nonlinear term in X exhibits a novel feature of being observationally favored over ΛCDM.

II. MODEL

We study the Galileon ghost condensate (GGC) model given by the action

$$S = \int d^4x \sqrt{-g} \left[\frac{M_{pl}^2}{2} R + a_1 X + a_2 X^2 + 3a_3 X \Box \phi \right] + S_M,$$
(1)

where $a_{1,2,3}$ are constants. For the matter action S_M, we consider perfect fluids minimally coupled to gravity. The existence of term $a_2 X^2$ leads to the modified evolution of w_{DE} and different cosmic growth history compared to those of the cubic Galileon (which corresponds to $a_2 = 0$). The ghost condensate model [31] can be recovered by taking the limit $a_3 \to 0$ in Eq. (1).

On the flat Friedmann-Lemaître-Robertson-Walker (FLRW) background given by the line element $ds^2 = -dt^2 + a^2(t)\delta_{ij}dx^i dx^j$, we consider nonrelativistic matter (density ρ_m with vanishing pressure) and radiation (density ρ_r and pressure $P_r = \rho_r/3$) for the action S_M. To discuss the background cosmological dynamics, it is convenient to introduce the dimensionless variables

$$x_1 = -\frac{a_1 \dot{\phi}^2}{3M_{pl}^2 H^2}, \quad x_2 = \frac{a_2 \dot{\phi}^4}{M_{pl}^2 H^2}, \quad x_3 = \frac{6a_3 \dot{\phi}^3}{M_{pl}^2 H}, \quad (2)$$

where $H = \dot{a}/a$, and a dot represents the derivative with respect to the cosmic time t. Then, the Friedmann equation can be expressed in the form $\Omega_m + \Omega_r + \Omega_{DE} = 1$ where $\Omega_m = \rho_m/(3M_{pl}^2 H^2)$, $\Omega_r = \rho_r/(3M_{pl}^2 H^2)$, and

$$\Omega_{DE} = x_1 + x_2 + x_3. \quad (3)$$

The variables x_1, x_2, x_3, and Ω_r correspond to density parameters associated with the Lagrangians $a_1 X$, $a_2 X^2$, $3a_3 X \Box \phi$, and radiation, respectively. Equation (3) evaluated today allows us to eliminate one free parameter, leaving the model with two extra parameters compared to ΛCDM.

The dynamical system can be expressed in the form

$$x_1' = 2x_1(\epsilon_\phi - h), \qquad x_2' = 2x_2(2\epsilon_\phi - h),$$
$$x_3' = x_3(3\epsilon_\phi - h), \qquad \Omega_r' = -2\Omega_r(2 + h), \quad (4)$$

where $\epsilon_\phi = \ddot{\phi}/(H\dot{\phi})$, $h = \dot{H}/H^2$, and a prime represents a derivative with respect to $\mathcal{N} = \ln a$. The explicit expressions of ϵ_ϕ and h are given in Eqs. (4.16) and (4.17) of Ref. [30] (with $x_4 = 0$). The dark energy equation of state is

$$w_{DE} = \frac{3x_1 + x_2 - \epsilon_\phi x_3}{3(x_1 + x_2 + x_3)}. \quad (5)$$

On the future de Sitter fixed point we have $\Omega_{DE} = 1$, and $w_{DE} = -1$ with $\epsilon_\phi = 0$, so there are two relations $x_1^{dS} = -2 + x_3^{dS}/2$ and $x_2^{dS} = 3 - 3x_3^{dS}/2$. Even though x_1^{dS} is negative for $x_3^{dS} \ll 1$, the ghost can be avoided by the positive x_2^{dS} term.

If the condition $x_3 \gg \{|x_1|, x_2\}$ is satisfied in the early cosmological epoch, we have $w_{DE} \simeq -\epsilon_\phi/3 \simeq 1/4 - \Omega_r/12 > 0$. On the other hand, in the limit $x_2 \to 0$, there exists a tracker solution satisfying the relation $x_3 = -2x_1$ (or equivalently, $\epsilon_\phi = -h$) [24, 30]. In this case, Eq. (5) reduces to $w_{DE} = -1 + 2h/3$ and hence $w_{DE} \simeq -2$ during the matter era. The existence of positive x_2 can lead to w_{DE} larger than -2, so the approach to the tracker is prevented by the term $a_2 X^2$. Indeed, after x_2 catches up with x_3, the solutions tend to approach the de Sitter attractor with x_3 subdominant to $|x_1|$ and x_2 at low redshifts [30]. In this way, the background dynamics temporally entering the region $-2 < w_{DE} < -1$ can be realized by the model (1) with $a_2 \neq 0$.

III. COSMOLOGICAL PERTURBATIONS

For the GGC model (1), the propagation of tensor perturbations is the same as that in General Relativity (GR). As for scalar perturbations, we consider the perturbed line element on the flat FLRW background:

$$ds^2 = -(1 + 2\Psi)dt^2 + a^2(t)(1 - 2\Phi)\delta_{ij}dx^i dx^j, \quad (6)$$

where Ψ and Φ are gravitational potentials. In Fourier space with the coming wavenumber k, we relate Ψ and $\Psi + \Phi$ with the total matter density perturbation $\rho\Delta = \sum_i \rho_i \Delta_i$ (where $i = m, r, ...$), as [32–34]

$$-k^2\Psi = 4\pi G_N a^2 \mu(a, k)\rho\Delta, \quad (7)$$
$$-k^2(\Psi + \Phi) = 8\pi G_N a^2 \Sigma(a, k)\rho\Delta, \quad (8)$$

where $G_N = (8\pi M_{pl}^2)^{-1}$ is the Newtonian gravitational constant. The dimensionless quantities μ and Σ characterize the effective gravitational couplings felt by matter and light, respectively. Applying the quasi-static approximation [35, 36] for perturbations deep inside the Hubble radius to the model (1), it follows that [30]

$$\mu = \Sigma = 1 + \frac{x_3^2}{Q_s c_s^2 (2 - x_3)^2}, \quad (9)$$

where

$$Q_s = \frac{3(4x_1 + 8x_2 + 4x_3 + x_3^2)}{(2 - x_3)^2}, \quad (10)$$

$$c_s^2 = \frac{2(1 + 3\epsilon_\phi)x_3 - x_3^2 - 4h - 6\Omega_m - 8\Omega_r}{3(4x_1 + 8x_2 + 4x_3 + x_3^2)}. \quad (11)$$

To avoid ghosts and Laplacian instabilities, we require that $Q_s > 0$ and $c_s^2 > 0$. Then, for $x_3 \neq 0$, μ and Σ are larger than 1, so both Ψ and $\Psi + \Phi$ are enhanced compared to those in GR. Since $\mu = \Sigma$, there is no gravitational slip ($\Psi = \Phi$). For the sub-horizon perturbations, the matter density contrast Δ approximately obeys

$$\ddot{\Delta} + 2H\dot{\Delta} - 4\pi G_N \mu \rho\Delta = 0, \quad (12)$$

so the cosmic growth rate is larger than that in GR. In the likelihood analysis, we solve full perturbation equations without resorting to the quasi-static approximation.

IV. METHODOLOGY OF COSMOLOGICAL PROBES

To confront the GGC model with observations, we use the Planck 2015 data of CMB temperature anisotropies and polarizations [5, 6]. For the Planck likelihood, we also vary the nuisance parameters exploited to model foregrounds as well as instrumental and beam uncertainties. We consider the former dataset in combination with data from the CMB lensing reconstruction [37], to which we refer as "Planck+Lensing". We include the BAO data from the 6dF galaxy survey [8] and the SDSS DR7 main galaxy sample [9]. Furthermore, we employ the combined BAO and RSD data from the SDSS DR12 consensus release [38], together with the JLA SNIa sample [3]. The latter dataset is called "PBRS".

We modify the public available Einstein-Boltzmann code EFTCAMB [39, 40] by implementing a background solver and mapping relations for the chosen model following the prescription in Refs. [41–44]. The built-in stability module allows us to identify the viable parameter space by imposing the two stability conditions $Q_s > 0$ and $c_s^2 > 0$. These results will be used to set priors for the data analysis. We impose flat priors on the initial values of two model parameters: $x_1^{(i)} \in [-10, 10] \times 10^{-16}$, $x_3^{(i)} \in [-10, 10] \times 10^{-9}$ at the redshift $z = 10^5$. We performed a test simulation in which the prior ranges are increased by one order of magnitude and found no difference for the likelihood results.

V. OBSERVATIONAL CONSTRAINTS

In Tables I and II, we show today's values $x_1^{(0)}, x_2^{(0)}, x_3^{(0)}$ and H_0, $\sigma_8^{(0)}$, $\Omega_m^{(0)}$ constrained from the Planck and PBRS datasets, together with bounds on the latter three parameters in ΛCDM. In Fig. 1, we also plot two-dimensional observational bounds on six parameters by including the Planck+Lensing data as well. In GGC, the Planck data alone lead to higher values of H_0 than that in ΛCDM. The former model is consistent with the Riess *et al.* bound $H_0 = 73.48 \pm 1.66$ km s^{-1} Mpc^{-1} derived by direct measurements of H_0 using Cepheids [11]. With the PBRS and CMB lensing datasets, we find that the bounds on H_0, $\sigma_8^{(0)}$ and $\Omega_m^{(0)}$ are compatible between GGC and ΛCDM. We do not include the data of direct measurements of H_0 and weak lensing, as they can be affected by the statistical analysis [45] and nonlinear perturbation dynamics [46], respectively.

The values of $x_1^{(0)}$ and $x_2^{(0)}$ constrained from the data are of order 1, with $x_1^{(0)} < 0$ and $x_2^{(0)} > 0$. We find the upper limit $x_3^{(0)} < 0.118$ (68 % CL) from the PBRS data. This bound mostly arises from the fact that the dominance of x_3 over x_2 at low redshifts leads to the enhanced Integrated Sachs-Wolfe (ISW) effect on CMB temperature anisotropies. The most stringent constraints on

Parameter	Planck	PBRS
$x_1^{(0)}$	$-1.27^{+0.22}_{-0.15}\,(-1.26)$	$-1.35^{+0.1}_{-0.07}\,(-1.27)$
$x_2^{(0)}$	$1.70^{+0.45}_{-0.73}\,(1.64)$	$1.95^{+0.18}_{-0.31}\,(1.74)$
$x_3^{(0)}$	$0.28^{+0.5}_{-0.3}\,(0.34)$	$0.09^{+0.2}_{-0.1}\,(0.23)$

Table I: Marginalized values of the model parameters $x_1^{(0)}, x_2^{(0)}, x_3^{(0)}$ and their 95% CL bounds, obtained by Planck and PBRS datasets. In parenthesis we show maximum likelihood values.

Parameter	Case	Planck	PBRS
H_0	GGC	$69.3^{+3.6}_{-3.0}\,(70)$	$68.1 \pm 1.1\,(68.4)$
	ΛCDM	$67.9 \pm 2.0\,(67.6)$	$68 \pm 1\,(68)$
$\sigma_8^{(0)}$	GGC	$0.86 \pm 0.04\,(0.87)$	$0.84 \pm 0.03\,(0.85)$
	ΛCDM	$0.841 \pm 0.03\,(0.83)$	$0.84 \pm 0.03\,(0.84)$
$\Omega_m^{(0)}$	GGC	$0.30 \pm 0.04\,(0.28)$	$0.305 \pm 0.01\,(0.30)$
	ΛCDM	$0.30 \pm 0.03\,(0.31)$	$0.31 \pm 0.01\,(0.31)$

Table II: Marginalized values of H_0, $\sigma_8^{(0)}$, $\Omega_m^{(0)}$ and their 95% CL bounds.

model parameters are obtained with the Planck+Lensing datasets. In Fig. 2, we plot the CMB TT power spectra for GGC as well as for ΛCDM and cubic Galileons (G3), given by the best-fit to the Planck data. The G3 model corresponds to $x_2 = 0$, so that the Galileon density is the main source for cosmic acceleration. In this case, the TT power spectrum for the multipoles $l < \mathcal{O}(10)$ is strongly enhanced relative to ΛCDM and this behavior is disfavored from the Planck data [27].

In GGC, the $a_2 X^2$ term in (1) can avoid the dominance of x_3 over x_2 around today. Even if $x_3^{(0)} \ll x_2^{(0)}$, the cubic
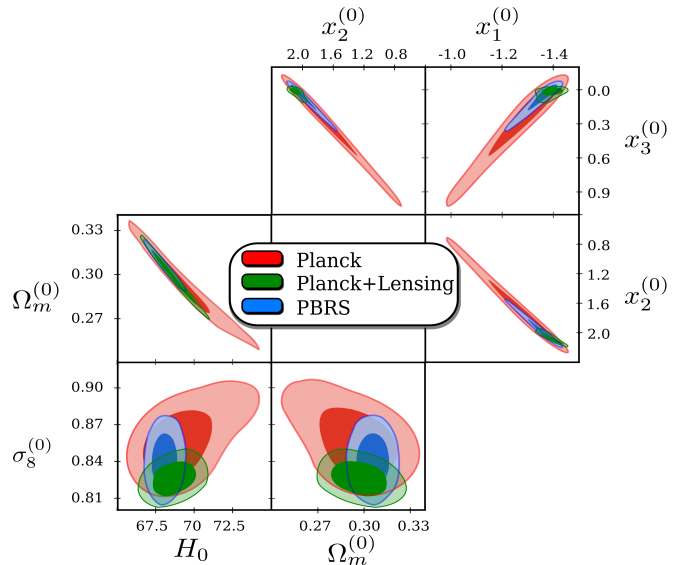

Figure 1: Joint marginalised constraints (68 % and 95 % CLs) on six model parameters $x_1^{(0)}, x_2^{(0)}, x_3^{(0)}, H_0, \sigma_8^{(0)}, \Omega_m^{(0)}$ obtained with the Planck, Planck+Lensing, and PBRS datasets.
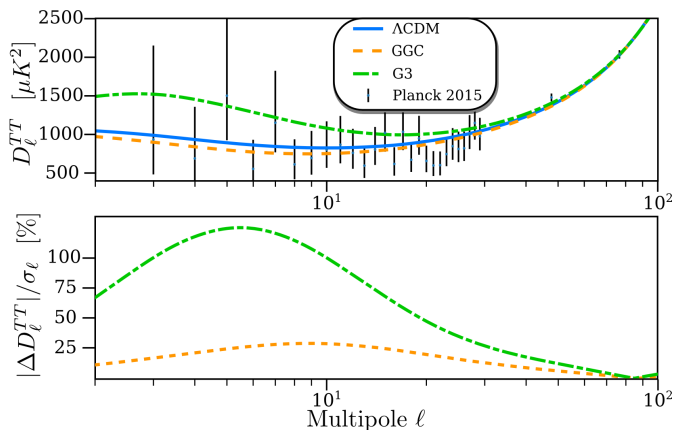
Figure 2: *Top panel*: Best-fit CMB temperature-temperature (TT) power spectra $D_\ell^{\mathrm{TT}} = \ell(\ell+1)/2\pi C_\ell^{\mathrm{TT}}$ at low multipoles ℓ for ΛCDM, GGC, and G3 (cubic Galileons), as obtained in the analysis of the Planck dataset. The best-fit values for G3 are taken from Ref. [27]. For comparison, we plot the data points from Planck 2015. *Bottom panel*: Relative difference of the best-fit TT power spectra, in units of cosmic variance $\sigma_\ell = \sqrt{2/(2\ell+1)} C_\ell^{\Lambda\mathrm{CDM}}$.
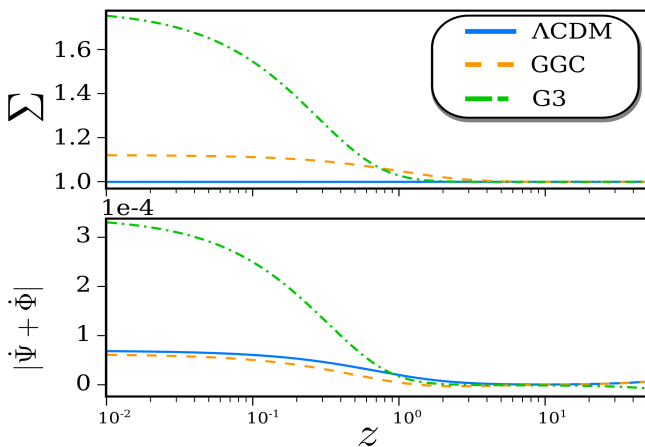
Figure 3: Best-fit evolution of Σ (top) and $|\dot\Psi + \dot\Phi|$ (bottom) versus z at $k = 0.01\ \mathrm{Mpc}^{-1}$ for ΛCDM, GGC, and G3 derived with the PBRS dataset.
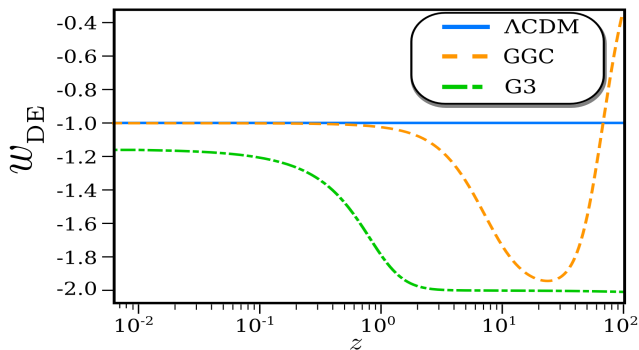

Figure 4: Best-fit evolution of w_{DE} versus z for ΛCDM, GGC, and G3 derived with the PBRS dataset.

Galileon gives rise to an interesting contribution to the CMB TT spectrum. As we see in Fig. 2, the best-fit GGC model is in better agreement with the Planck data relative to ΛCDM by suppressing large-scale ISW tails. Taking the limit $x_3^{(0)} \to 0$, the TT spectrum approaches the one in ΛCDM. The TT spectrum of G3 in Fig. 2 can be recovered by taking the limit $x_3^{(0)} \gg x_2^{(0)}$.

In Fig. 3, we depict the evolution of Σ and $|\dot\Psi + \dot\Phi|$ for GGC, G3 and ΛCDM, obtained from the PBRS best-fit. In G3, the large growth of Σ from 1 leads to the enhanced ISW effect on CMB anisotropies determined by the variation of $\Psi + \Phi$ at low redshifts. For the best-fit GGC, the deviation of Σ from 1 is less significant, with $\dot\Psi + \dot\Phi$ closer to 0. In the latter case, the TT spectrum is suppressed with respect to ΛCDM. This is why the intermediate value of $x_3^{(0)}$ around 0.1 with $x_2^{(0)} = \mathcal{O}(1)$ exhibits the better compatibility with the CMB data relative to ΛCDM.

As we see in Fig. 4, the best-fit GGC corresponds to the evolution of w_{DE} approaching the asymptotic value -1 from the region $-2 < w_{\mathrm{DE}} < -1$. This overcomes the problem of G3 in which the $w_{\mathrm{DE}} = -2$ behavior during the matter era is inconsistent with the CMB+BAO+SNIa data [25]. This nice feature of w_{DE} in GGC again comes from the combined effect of x_2 and x_3.

VI. MODEL SELECTION

The GGC model has two extra parameters with respect to ΛCDM, to allow for a better fit to the data. In order to determine whether GGC is favored over ΛCDM, we make use of the Deviance Information Criterion (DIC) [47]:

$$\mathrm{DIC} = \chi_{\mathrm{eff}}^2(\hat\theta) + 2p_{\mathrm{D}}, \qquad (13)$$

where $\chi_{\mathrm{eff}}^2(\hat\theta) = -2\ln\mathcal{L}(\hat\theta)$ with $\hat\theta$ being parameters maximizing the likelihood function $\mathcal{L}$, and $p_{\mathrm{D}} = \bar\chi_{\mathrm{eff}}^2(\theta) - \chi_{\mathrm{eff}}^2(\hat\theta)$. Here, the bar denotes an average over the posterior distribution. We observe that the DIC accounts for both the goodness of fit, $\chi_{\mathrm{eff}}^2(\hat\theta)$, and for the Bayesian complexity of the model, p_{D}, which disfavors more complex models. For the purpose of model comparisons, we compute

$$\Delta\mathrm{DIC} = \mathrm{DIC}_{\mathrm{GGC}} - \mathrm{DIC}_{\Lambda\mathrm{CDM}}, \qquad (14)$$

from which we infer that a negative (positive) $\Delta\mathrm{DIC}$ would support GGC (ΛCDM).

We also consider the Bayesian evidence factor ($\log_{10} B$) along the line of Refs. [48, 49] to quantify the support for GGC over ΛCDM. A positive value of $\Delta\log_{10} B$ indicates a statistical preference for the extended model and a strong preference is defined for $\Delta\log_{10} B > 2$.

In Table III, we list the values of $\Delta\chi_{\mathrm{eff}}^2$, $\Delta\mathrm{DIC}$ and $\Delta\log_{10} B$ computed with respect to ΛCDM for each dataset considered in this analysis. For Planck and PBRS

Dataset	$\Delta\chi^2_{\text{eff}}$	ΔDIC	$\Delta\log_{10}B$
Planck	−4.8	−2.5	4.4
PBRS	−2.8	−0.6	5.1
Planck+Lensing	−0.9	0.80	1.6

Table III: Model comparisons through the obtained values of $\Delta\chi^2_{\text{eff}}$, ΔDIC and $\Delta\log_{10}B$ using ΛCDM as reference.

both ΔDIC and $\Delta\log_{10}B$ exhibit significant preferences for GGC over ΛCDM. This suggests that not only the CMB data but also the combination of BAO, SNIa, RSD datasets favors the cosmological dynamics of GGC like the best-fit case shown in Figs. 3 and 4. With the Planck+Lensing data the χ^2_{eff} and Bayesian factor exhibit slight preferences for GGC, while the DIC mildly favours ΛCDM. The model selection analysis with the CMB lensing data does not give a definite conclusion for the preference of models. We note that, among the likelihoods used in our analysis, the CMB lensing alone assumes ΛCDM as a fiducial model [37]. This might source a bias towards the latter.

VII. CONCLUSION

We have shown that, according to the two information criteria, GGC is significantly favoured over ΛCDM with the PBRS datasets. This property holds even with two additional model parameters than those in ΛCDM. According to our knowledge, there are no other scalar-tensor dark energy models proposed so far showing such novel properties. This surprising result is attributed to

the properties that, for $x_3^{(0)} \ll x_2^{(0)} = \mathcal{O}(1)$, (i) suppressed ISW tails relative to ΛCDM can be generated, and (ii) w_{DE} can be in the region $-2 < w_{\text{DE}} < -1$ at low redshifts. The GGC model deserves for being tested further in future observations of WL, ISW-galaxy cross-correlations, and gravitational waves.

[1] A. G. Riess *et al.*, Astron. J. **116**, 1009 (1998).
[2] S. Perlmutter *et al.*, Astrophys. J. **517**, 565 (1999).
[3] M. Betoule *et al.*, Astron. Astrophys. **568**, A22 (2014).
[4] D. N. Spergel *et al.*, Astrophys. J. Suppl. **148**, 175 (2003).
[5] P. A. R. Ade *et al.*, Astron. Astrophys. **594**, A13 (2016).
[6] N. Aghanim *et al.*, Astron. Astrophys. **594**, A11 (2016).
[7] D. J. Eisenstein *et al.*, Astrophys. J. **633**, 560 (2005)
[8] F. Beutler *et al.*, Mon. Not. Roy. Astron. Soc. **416**, 3017 (2011).
[9] A. J. Ross *et al.*, Mon. Not. Roy. Astron. Soc. **449**, 835 (2015).
[10] S. Weinberg, Rev. Mod. Phys. **61**, 1 (1989).
[11] A. G. Riess *et al.*, Astrophys. J. **861**, no. 2, 126 (2018).
[12] G. W. Horndeski, Int. J. Theor. Phys. **10**, 363 (1974).
[13] C. Deffayet, X. Gao, D. A. Steer and G. Zahariade, Phys. Rev. D **84**, 064039 (2011).
[14] T. Kobayashi, M. Yamaguchi and J. Yokoyama, Prog. Theor. Phys. **126**, 511 (2011).
[15] B. P. Abbott *et al.*, Phys. Rev. Lett. **119**, 161101 (2017).
[16] A. Goldstein *et al.*, Astrophys. J. **848**, L14 (2017).
[17] T. Baker, E. Bellini, P. G. Ferreira, M. Lagos, J. Noller and I. Sawicki, Phys. Rev. Lett. **119**, 251301 (2017).
[18] P. Creminelli and F. Vernizzi, Phys. Rev. Lett. **119**, 251302 (2017).

[19] J. Sakstein and B. Jain, Phys. Rev. Lett. **119**, 251303 (2017).
[20] J. M. Ezquiaga and M. Zumalacarregui, Phys. Rev. Lett. **119**, 251304 (2017).
[21] L. Amendola, M. Kunz, I. D. Saltas and I. Sawicki, Phys. Rev. Lett. **120**, 131101 (2018).
[22] A. Nicolis, R. Rattazzi and E. Trincherini, Phys. Rev. D **79**, 064036 (2009).
[23] C. Deffayet, G. Esposito-Farese and A. Vikman, Phys. Rev. D **79**, 084003 (2009).
[24] A. De Felice and S. Tsujikawa, Phys. Rev. Lett. **105**, 111301 (2010).
[25] S. Nesseris, A. De Felice and S. Tsujikawa, Phys. Rev. D **82**, 124054 (2010).
[26] J. Renk, M. Zumalacaregui, F. Montanari and A. Barreira, JCAP **1710**, 020 (2017).
[27] S. Peirone, N. Frusciante, B. Hu, M. Raveri and A. Silvestri, Phys. Rev. D **97**, 063518 (2018).
[28] A. Ali, R. Gannouji, M. W. Hossain and M. Sami, Phys. Lett. B **718**, 5 (2012)
[29] R. Kase, S. Tsujikawa and A. De Felice, Phys. Rev. D **93**, 024007 (2016).
[30] R. Kase and S. Tsujikawa, Phys. Rev. D **97**, 103501 (2018).

[31] N. Arkani-Hamed, H. C. Cheng, M. A. Luty and S. Mukohyama, JHEP **0405**, 074 (2004).

[32] L. Amendola, M. Kunz and D. Sapone, JCAP **0804**, 013 (2008).

[33] E. Bertschinger and P. Zukin, Phys. Rev. D **78**, 024015 (2008).

[34] L. Pogosian, A. Silvestri, K. Koyama and G. B. Zhao, Phys. Rev. D **81**, 104023 (2010).

[35] B. Boisseau, G. Esposito-Farese, D. Polarski and A. A. Starobinsky, Phys. Rev. Lett. **85**, 2236 (2000).

[36] A. De Felice, T. Kobayashi and S. Tsujikawa, Phys. Lett. B **706**, 123 (2011).

[37] P. A. R. Ade *et al.* [Planck Collaboration], Astron. Astrophys. **594**, A15 (2016).

[38] S. Alam *et al.*, Mon. Not. Roy. Astron. Soc. **470**, 2617 (2017).

[39] B. Hu, M. Raveri, N. Frusciante and A. Silvestri, Phys. Rev. D **89**, 103530 (2014).

[40] M. Raveri, B. Hu, N. Frusciante and A. Silvestri, Phys. Rev. D **90**, 043513 (2014)

[41] G. Gubitosi, F. Piazza and F. Vernizzi, JCAP **1302**, 032 (2013).

[42] J. K. Bloomfield, E. E. Flanagan, M. Park and S. Watson, JCAP **1308**, 010 (2013).

[43] J. Gleyzes, D. Langlois, F. Piazza and F. Vernizzi, JCAP **1308**, 025 (2013).

[44] N. Frusciante, G. Papadomanolakis and A. Silvestri, JCAP **1607**, 018 (2016).

[45] G. Efstathiou, Mon. Not. Roy. Astron. Soc. **440**, 1138 (2014).

[46] H. Hildebrandt *et al.*, Mon. Not. Roy. Astron. Soc. **465**, 1454 (2017).

[47] D. J. Spiegelhalter, N. G. Best, B. P. Carlin, and A. van der Linde, J. Roy. Statist. Soc. B **76**, 485 (2014).

[48] A. Heavens *et al.*, arXiv:1704.03472.

[49] F. De Bernardis, T. D. Kitching, A. Heavens and A. Melchiorri, Phys. Rev. D **80**, 123509 (2009).